NEW OPTICAL NAVIGATION RESULTS USING HISTORICAL MESSENGER DATA

Vaishnavi V. Ramanan[1,2*], Michael A. Shoemaker[1], and Andrew J. Liounis[1]; [1]NASA Goddard Space Flight Center, Greenbelt, MD 20771, [2]Georgia Institute of Technology, Atlanta, GA 30332 *[vaish@gatech.edu]

Abstract. *This paper describes new optical navigation (OpNav) results obtained by processing previously collected measurements from the MESSENGER mission to Mercury. This project also serves to mature the tools and capabilities of NASA Goddard Space Flight Center (GSFC) in OpNav, using the open source Goddard Image Analysis and Navigation Tool (GIANT). New navigation measurements are obtained during the Mercury flyby and orbital phases, using OpNav measurements generated by GIANT, and these measurements are compared to predictions. The results obtained provide a set of improvements to be made in navigation tools and will pave the way for future missions to navigate near terrestrial bodies using optical measurements.*

Introduction. Optical Navigation (OpNav) is the process of using in situ images of celestial bodies to aid in determining target ephemerides and spacecraft trajectories. In this paper, we focus on Terrain Relative Navigation (TRN) using surface feature measurements. TRN, also called Surface Feature Navigation (SFN), is the process of utilizing a map-relative state estimation, with applications that include the precision landing and hazard avoidance on a planetary surface. This process makes use of images of terrain on surfaces of celestial targets and compares unique surface features to that of *a priori* maps (previously collected images or derived Digital Terrain Models (DTMs)), resulting in line-of-sight (LOS) measurements. TRN can be used in many phases of mission operations, including flybys, survey and orbital phases, and entry, descent, and landing activities. TRN is used to reduce spacecraft state uncertainties (when the spacecraft is relatively close to the targeted body) and is typically performed as part of the overall orbit determination process[1].

While traditional radiometric tracking methods via the Deep Space Network (DSN), such as sequential range and Doppler, can be directly observed with high precision in the radial direction with respect to the ground station, the along and cross-track directions must be inferred using *a priori* knowledge of the spacecraft dynamics (with an error range from tens to thousands of meters)[2]. Although other DSN observables (such as ΔDOR) can reduce these plane-of-sky uncertainties, they require specialized support and are more difficult to schedule, as two DSN stations must be simultaneously available. There are other limitations of using radiometric tracking methods in some situations, including Doppler measurement phase scintillation during periods of the year when Sun-Earth-probe angles are small, decreasing the accuracy of Doppler measurements significantly. To mitigate levels of error in navigation, making use of OpNav in combination with traditional radiometric measurements is necessary for some mission concepts.

The Mercury, Surface, Space Environment, Geochemistry, and Ranging (MESSENGER) mission was the 7th mission in NASA's Discovery Program, spanning from 2004 to 2015, and was managed by Johns Hopkins University Applied Physics Laboratory (JHU/APL)[3]. With an objective of characterizing the geology, magnetic field, and chemical composition of the planet, the space probe arrived at the planet through multiple planetary flybys and Deep-Space Maneuvers (DSMs). Mission Design and Navigation Teams at JHU/APL and KinetX Aerospace, respectively, performed orbit determination, Trajectory Correction Maneuver (TCM) reconstruction, design, and optimization using the following DSN radiometric data types: two-way Doppler, three-way Doppler, two-way ranging, and ΔDOR. Ground-based OpNav was also utilized on MESSENGER during the first Mercury gravity assist using narrow field-of-view (FOV) images, primarily to reduce Mercury ephemeris uncertainty in support of the contingency TCM scheduled for 34 hours prior to close approach[4]. Despite restrictions, the processing went well and revealed issues in the navigation solution that were addressed in subsequent flybys. However, the Mercury orbital phase of the mission did not use OpNav measurements[4]. One complication to using OpNav measurements was the fact that the MESSENGER spacecraft used a gimbaled instrument platform called the Mercury Dual Imaging System (MDIS) to point its cameras to different targets on the surface, hence precise camera pointing knowledge can be more difficult to obtain compared with a stationary platform.

In addition to the narrow FOV camera data collected during the flybys, a large number of wide FOV images were collected at close approach and during the orbital phase. Although not originally used for OpNav on the mission, this data was used to generate detailed surface DTMs and achieve other science objectives. The MESSENGER images and DTM data are currently published to the Planetary Data System (PDS)[5], with best-fit navigation results also available on the Navigation and Ancillary Information Facility (NAIF)[6]. The OpNav data from this mission is used to accomplish specific objectives mentioned in the next section.

Motivation and Objectives. This paper describes the results of a GSFC effort with the objective of maturing the tools and processes for performing OpNav. The focus of this effort is the open source Goddard Image Analysis

and Navigation Tool (GIANT), developed at GSFC[7,8]. Another motivation for this work is to evaluate whether the global 665-m resolution Mercury DTM[9] is suitable for performing SFN, as the typical OpNav process performed on other past missions would first use sterephotoclinometry (SPC) to build up a large set of high-resolution terrain features. In contrast, starting from a global DTM (not necessarily originally intended for OpNav), may shed light on the usefulness of using this analysis pipeline to support future OpNav operations at planetary bodies where a global DTM already exists (e.g. the Moon).

GIANT is a suite of Python tools capable of performing functions including camera calibration and OpNav (through far-field centroiding, limb-scanning, and SFN) and was successfully used on OSIRIS-REx for independent navigation analysis during proximity operations at the near-Earth asteroid (101955) Bennu[2]. The far-field centroiding and limb-matching functions of GIANT involves identifying limb points in the image using modern image processing edge detection techniques, matching these points from the image to predicted limb points from a shape model of the given target, and providing an updated or final solution for the center-of-figure of the target in the image[11].

This project represents an innovative use of existing mission data from MESSENGER to obtain new navigation results using GIANT. This application to the MESSENGER Mercury flybys and orbital phase represents one of the first examples where GIANT has been used during planetary flyby or orbital phases (as opposed to small body operations) and will further refine its capabilities in the OpNav domain. A secondary objective of this project is to provide a set of baseline planetary navigation results for future validation of autonomous flight software.

Methodology. Several steps must be taken to meet the stated objectives. First, images from two phases of the MESSENGER mission – Mercury Gravity Assist 1 and Science Orbit 1 – are acquired using the PDS Image Atlas. Next, the global DTM is processed to create a set of surface features that are predicted to be within these images as landmarks of interest. GIANT processes these surface features to create LOS measurements between the camera and the landmark. Ultimately, a navigation filter would be used to process the LOS measurements and create ephemeris files (and uncertainty estimates) of the spacecraft state, which can be compared with definitive best-fit ephemerides from NAIF. As an intermediate step, the global DTM is interpolated and SPC maplets are generated, which are then converted into surface features that are ingested by GIANT. The next section describes this process of generating SPC maplets from the global DTM.

Creating Maplets. A *maplet* is the small subset of terrain, or topography, for the corresponding region around the landmark[12]. There are several elements used to create a maplet, which differentiates it from a subset of a DTM. These elements are listed as follows:

- *Maplet Grid Resolution*: The number of grid elements specifying the size of the grid, usually defined as *(N x N)* in size. The maplets used in this project are of size *199 x 199* (39601 total points)
- *Maplet Grid Scale*: Equivalent to the Ground Sample Distance (GSD) of that within a user-specified image
- *Landmark*: Body-fixed center (origin) vector of the maplet - not referring to the terrain around the origin but the coordinate itself
- *Rotation matrix from Local Maplet Frame to the Body-Fixed Frame*: Rotation from the local maplet coordinate frame (with z-axis pointing zenith and centered on landmark) to body-fixed frame
- *2D Matrix of Heights*: The height profile for the maplet as an *N x N* array
- *2D Matrix of Albedos*: The albedo profile, or amount of light reflected from the surface, for the maplet as an *N x N* array

The maplet creation pipeline used for this project consists of several steps, intended to fill each element of the maplet class. The required inputs for this pipeline are listed as follows:

- A geoTIFF DTM - Global Mercury DTM with 665 meter resolution
- Images of the target body surface containing visible surface features
- Image associated label files containing information specifying image time, size, and center coordinates; horizontal and vertical pixel scale; and slant distance from camera to surface
- Camera Specifications including focal length and pixel pitch
- Spacecraft SPICE kernels specifying spacecraft and target body position and velocity, and camera orientation

With all inputs specified, the maplet creation process within the pipeline, including the input acquisition process, can be described. First, images acquired from the PDS are used in identifying noticeable landmarks. Images are initially sorted based on individual Ground Sample Distance (GSD). GSD is the distance between the center of consecutive image pixels as measured on the surface, and is a function of the following elements:

$$GSD = \frac{Slant\ Distance * Camera\ Pixel\ Pitch}{Focal\ Length}$$

The average GSD for the science orbit phase was approximately 2 km, and the flyby phase was between 2

and 3 km. Therefore, the required maplet GSD was within a scale factor of approximately 2 to 3 with respect to the input global DTM with a 665-m resolution.

The foundation for creating Mercury maplets is the global DTM of Mercury published on PDS, with a resolution of 665 meters per pixel. To ensure more accurate results during the SFN processing in GIANT, images are sorted such that each image GSD is close in value to the global DTM resolution. Images are then manually sorted based on the variety of terrain and presence of noticeable surface features. Maplets with little variation in terrain, such as flat land, are difficult test cases to use when compared to images as pixels are similar across the test section. Note that the albedo in each maplet was set to a constant value of 0.5 as a simplifying assumption, to avoid the added complexity of needing to process albedo data of the Mercury surface from PDS. In practice, using a constant albedo does not significantly affect the SFN correlation step, assuming there is sufficient terrain relief (i.e. elevation variation) and the incidence angle is not near-zero[13].

The next step in the process involves acquiring label files associated with the images from the PDS, specifying elements like image time, slant distance, camera specifications, and center coordinates (in latitude and longitude). Based on a user-specified image, the associated label file with the image time is pulled, and the MESSENGER SPICE kernel specifications are narrowed to the image time.

To trace the camera bounds and any user-specified landmarks at image time (resulting in latitude and longitude coordinates), the **ray_tracer** subpackage in GIANT is used. Ray tracing is the process of tracing light backwards from the camera to a light source[2]. Rays from a model of the camera are traced from the camera to a model of the surface of Mercury to find where the rays intersect with topography. This process results in a visualization of the camera bounds along with any user-specified landmarks identified through the selection of image pixel row and column values. These pixel values are projected down to the modeled surface of Mercury to find each landmark coordinate

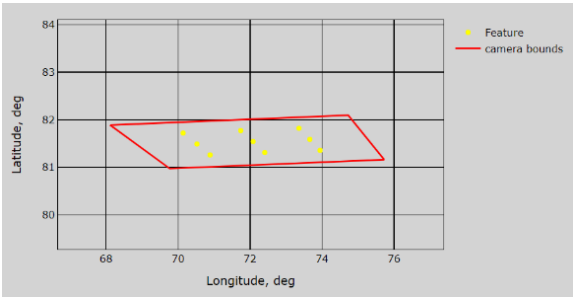

Figure 1. Model of MESSENGER camera bounds and 9-point grid of landmarks shown on Latitude/Longitude map

Last, landmark coordinates are interpolated to the global Mercury DTM. The DTM is transformed from geoTIFF image coordinates[14] to geographic coordinates, using the GDAL python library[15], and the terrain is cropped around each landmark. This cropped DTM provides information to fill the maplet element of 2D matrix of heights. With all maplet elements specified, the GIANT Maplet class is populated to create and visualize sets of maplets for two phases of the MESSENGER mission, as shown in *Figures 2 and 3*. Once all the SPC-formatted maplet files are generated, they are converted into surface feature format to be ingested into GIANT.

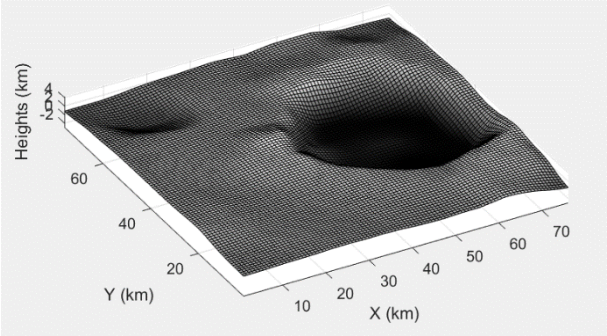

Figure 2. Maplet visualization, with specified landmark as origin of the maplet

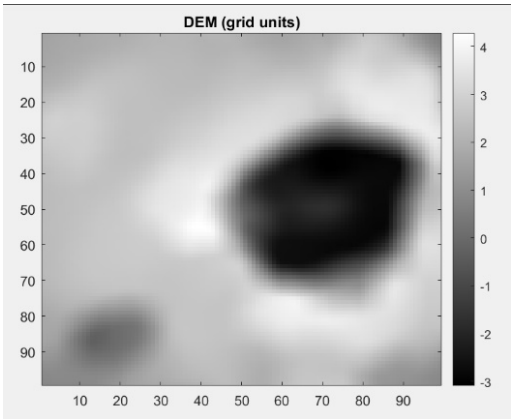

Figure 3. Maplet mesh grid visualization in grid units

GIANT Surface Feature Nav. The remaining step is to use GIANT's SFN functionality to render the predicted template for each surface feature, and correlate that template to the predicted surface feature location in the image, producing the updated image (col, row) coordinates for the LOS measurement. As mentioned above, we use SPICE kernels to model the state of the spacecraft, camera, and planet. The current study uses the most recent SPICE kernels published by the MESSENGER project, that include updated attitude and camera calibration. Hence, we are not trying to reproduce a navigation process using the information known at the time of the actual mission operations. In contrast, we are

taking advantage of the best reconstructed data that is available at the present time. This assumption is justified because the goal of the present study is an analysis of GIANT measurement performance and its dependence on landmark rendering and correlation. Although *a priori* uncertainties in camera pose will also affect these results, addressing the magnitude of these uncertainties and ways to address them is left as future work. The minimum allowable correlation score was set to the extreme limit of -1 to prevent throwing away any measurements, in order to examine the effect of landmark selection on the correlation score. Although -1 is the theoretical lower limit from a mathematical sense, a more reasonable practical limit for future analysis would be 0 or 0.1.

Science Orbit Results. A portion of the science orbit was selected to test the above-mentioned surface feature measurement generation process in GIANT. For this preliminary analysis, we restrict ourselves to WAC un-binned images. The implementation of the NAC camera model required further modifications to GIANT which were outside the scope of the current paper. The primary science orbit from March 2011 to March 2012 included an MDIS imaging campaign for generating a global morphology map, which included WAC images at both high and low latitudes[16]. We filtered the PDS images during this morphology campaign to those images having incidence angles at the camera boresight near ~60 degrees, and using the "F" WAC filter (433 nm wavelength, denoted WAC-F). In general, there were not noticeable differences (from a navigation standpoint) when using WAC images having different filters; limiting our results to a single filter was a way to reduce extraneous images collected from nearly the same time instant and vantage point in the orbit. The resulting science orbit WAC-F images for the current experiments spanned dates from 3/29/2011 to 4/20/2011, numbering 157 images (see Figure 4 for one example image).

In each WAC-F image, we defined a 3x3 grid of points evenly spread in the image (as described in Figure 1). These 9 landmarks were then generated using the above-described interpolation of the global 665-m resolution DTM, and then only applied to the current image. Note that although this approach is simple to implement, it ignores the information content in the surface terrain when choosing landmarks, and therefore is prone to generating landmarks with low correlation scores (to be discussed below). Also note that if a landmark was placed in a region of local night (incidence angle > 90 deg), it was rejected. Because some WAC-F images from different times along the science orbit overlapped the same region on the surface, this surface feature generation scheme is inherently inefficient, as surface features from a given image are not reused in later images. However, because the focus of the current study was on analyzing the usefulness of MESSENGER MDIS data for performing SFN, we preferred to have an overabundance of test data. Figure 5 shows the resulting landmark locations in latitude and longitude; it is clear that most landmarks occur at latitude near the south pole, because that is the region of Mercury visible to full-frame WAC-F images near apoapsis, given the science orbit periapsis location near the north pole.

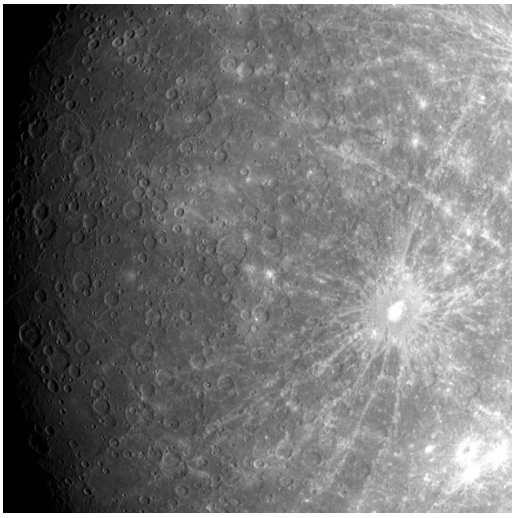

Figure 4. Example WAC-F image from selected science orbit date range, where GSD at the boresight is 2.7 km/pixel .

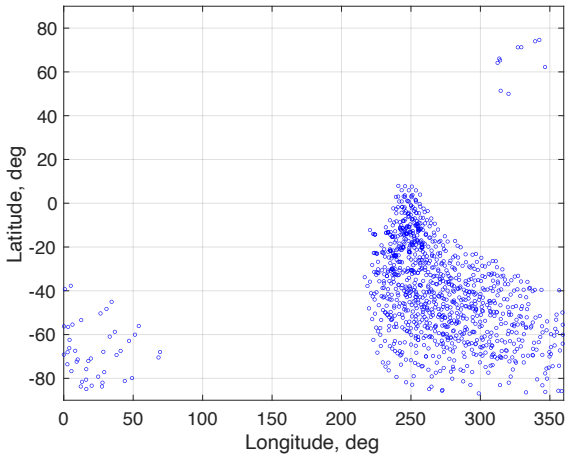

Figure 5. Science orbit landmark locations during 3/29/2011 to 4/20/2011 test span.

Figure 6 shows the results of processing the set of science orbit images in GIANT's SFN functions. We treat these differences as "errors" for the purposes of discussion, although strictly speaking the measurement model parameters (e.g. spacecraft state, camera model, surface DTM model), on which the predicted and measurement values are dependent, are not perfectly known, therefore there is no concept of "truth". The

distribution of errors in Figure 6 shows a mean (col, row) error of (1.6, -0.5) pixels, and a standard deviation of (0.75, 0.95) pixels. Having a standard deviation below 1 pixel in the (col, row) components indicates that these SFN measurements are suitable for inclusion in a navigation filter as future work. The presence of an apparent bias could be a reflection of the increased MDIS instrument pointing uncertainty caused by the gimballed platform, or other details of our implementation that are yet to be determined.

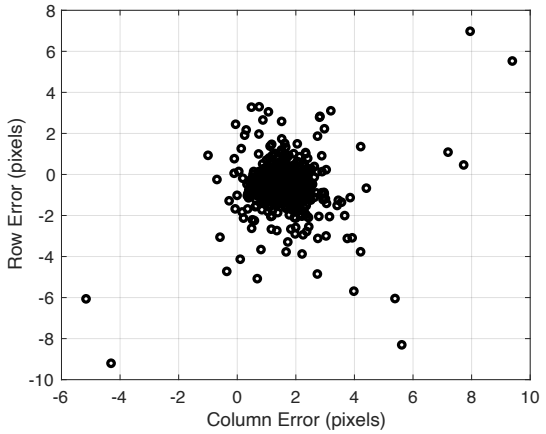

Figure 6. SFN landmark measurement column and row pixel error during science orbit test span.

Because the landmarks were placed on the surface without regard for information content in the terrain relief, and because GIANT was configured to allow the full range of correlation scores from -1 to 1, it is not surprising to see a wide variation in resulting correlation score in each measurement (Figure 7). However, we do not see a strong dependence on measurement error to correlation score. Although our randomly selected landmarks were largely able to generate measurements with consistent error statistics, this result should serve as a motivation for future autonomous systems; careful selection of landmarks and a higher threshold on the correlation score will nonetheless reduce the likelihood of false correlations. In practice, a lower correlation score limit of 0.6 is recommended, which is reflected in Figure 7 by the lack of outliers above this value.

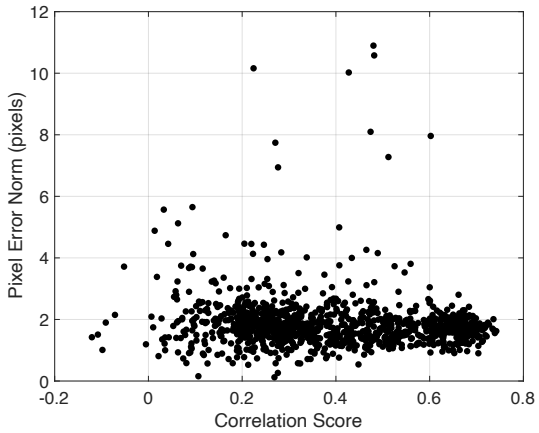

Figure 7. Science orbit peak measurement error (norm) vs. correlation score.

We can examine plots of the correlation score vs incidence angle (Figure 8) and emission angle (Figure 9) to gain more insight into what conditions result in a landmark with a higher correlation score. Figure 8 shows that incidence angles around 55 to 75 deg results in the highest correlation (in terms of max value and the moving-mean line shown in blue). This result is likely due to two reasons: (1) The morpohology imaging campaign used WAC-G and NAC images having a similar range of incidence angles to generate the DTM. Therefore, the features in the 665-m DTM topology could be inherently biased to appear "better" when rendered at these incidence angles. (2) Because our surface features do not contain albedo, low incidence angles cause a loss of recognizable features. Figure 9 shows an aliasing in the data that results from the 3 x 3 grid of rays for determining landmark location, i.e. the center grid rays will always have low emission angles, and the edge grid rays will always have ~20 to ~30 deg emission angles. Despite this aliasing, we can see that emission angle does not appear to be a strong predictor for correlation score performance, because the groupings of data have a similar spread in correlation value.

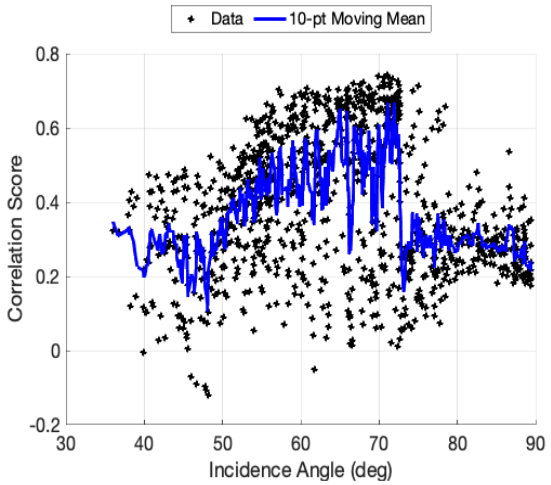

Figure 8. Science orbit landmark correlation score vs. incidence angle.

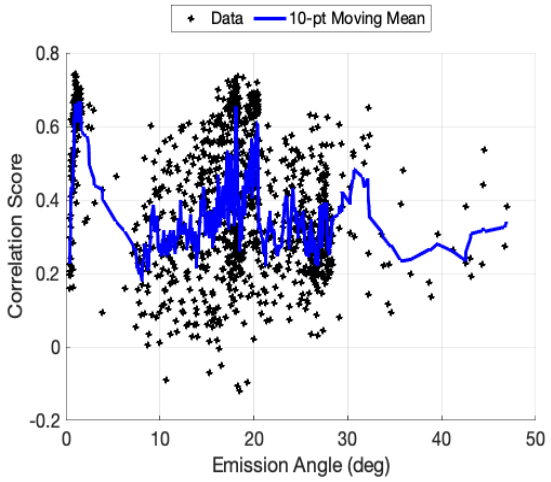

Figure 9. Science orbit landmark correlation score vs. emission angle.

First Mercury Flyby Results:

Because the flyby happens relatively quickly (compared with the science orbit phase analyzed above), there were fewer un-binned WAC-F images available for analysis. Table 1 shows the eleven resulting images, where the first image is approximately 2 hours before closest approach ("arrival"), the last image is approximately 1 hour after closest approach ("departure"), and the remaining images are all within approximately one minute of each other near closest approach. A selection of these images is shown in Figure 10, where the number denoted in the image matches the first column in Table 1. The "arrival" image (#1) and the "departure" image (#11) show Mercury in a full frame, and the remaining images are collected in a MDIS scanning pattern designed to create a mosaic.

Table 1. Timeline of WAC-F images used for SFN tests of 1st Mercury Flyby.

Num.	Image Name	Image Start Time
1	CW0108820022F_RA_5	2008-01-14 17:44:01
2	CW0108827293F_RA_5	2008-01-14 19:45:12
3	CW0108827370F_RA_5	2008-01-14 19:46:29
4	CW0108827407F_RA_5	2008-01-14 19:47:06
5	CW0108827546F_RA_5	2008-01-14 19:49:25
6	CW0108827623F_RA_5	2008-01-14 19:50:42
7	CW0108827660F_RA_5	2008-01-14 19:51:19
8	CW0108827799F_RA_5	2008-01-14 19:53:38
9	CW0108827876F_RA_5	2008-01-14 19:54:55
10	CW0108827913F_RA_5	2008-01-14 19:55:32
11	CW0108829713F_RA_5	2008-01-14 20:25:32

The landmarks for the flyby were generated using the same analysis pipeline as described above, with the one main difference being the manual selection of approximately 15 to 30 landmarks per image, as opposed to the 3x3 fixed grid of ray intersections to the surface that was used for the science orbit tests. The landmarks were selected by viewing each image and selecting pixel coordinates that corresponded to visual features (e.g. crater groupings), without a preference for local incidence or emission angle. This manual landmark selection process was used to ensure a large enough data set, given that there were only eleven images to work with. Figure 11 shows the resulting landmark latitudes and longitudes, where blue denotes the arrival image, black denotes the mosaic scan around closest approach, and red denotes the departure image, which further illustrates the limited nature of the WAC data for this flyby.

Figure 12 shows the corresponding column and row pixel errors after the GIANT SFN process has been run, where again the color annotations show arrival, close approach, and departure. Unlike the science orbit results in Figure 6, now we see a bifurcation in the distribution, with the errors clustering around two biased values. The fact that the blue and red points do not cross the clusters, and that the black points from the mosaic scan occupy both clusters, suggests the bias could be associated with a variable MDIS gimbal location. Despite the presence of an apparent bias, the variance in the points is in-family with Figure 6, with a standard distribution for each set of approximately 1 pixel in each component. Therefore, this test demonstrates that OpNav SFN measurements during the flyby could potentially be useful for ingesting into the navigation filter, despite only having a limited set of data. The biggest hurdle to overcome is reducing the apparent bias, or mitigating it using other means (e.g. estimating the bias as a stochastic parameter or including as a consider parameter).

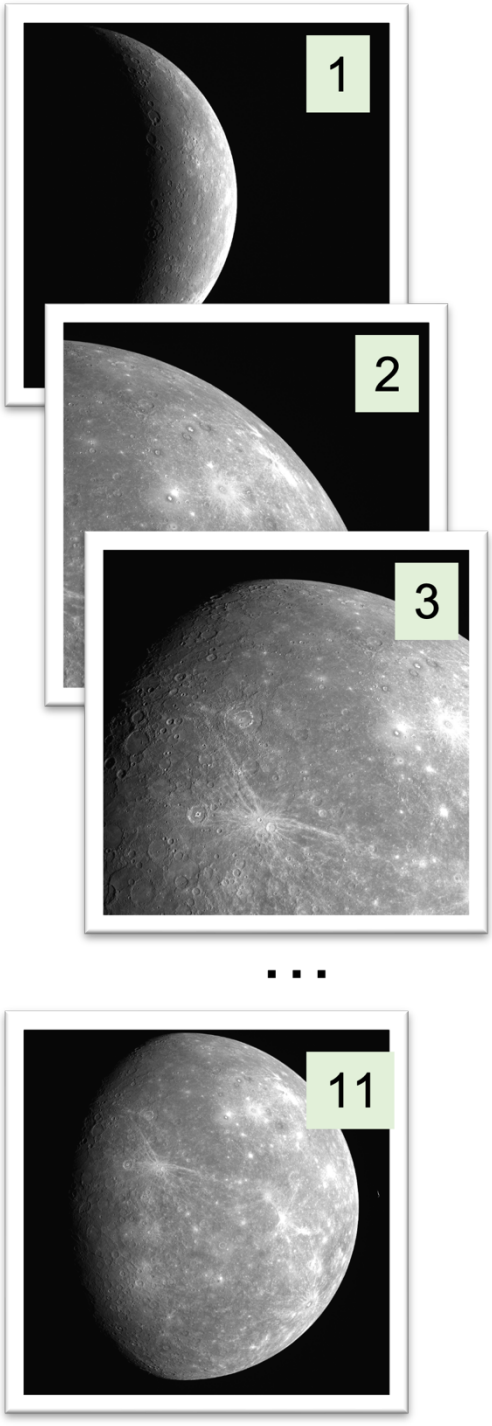

Figure 10. Selection of Mercury Flyby 1 images, where number annotation corresponds to Table 1.

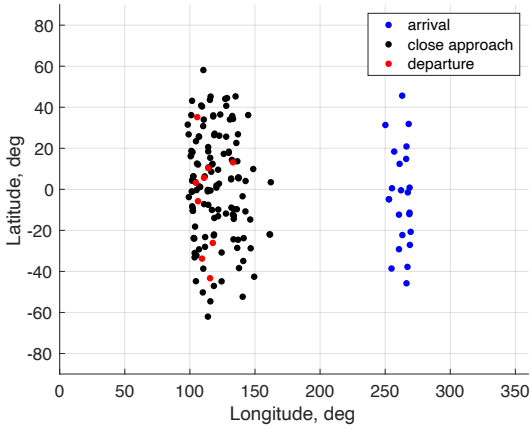

Figure 11. First Mercury flyby landmark locations.

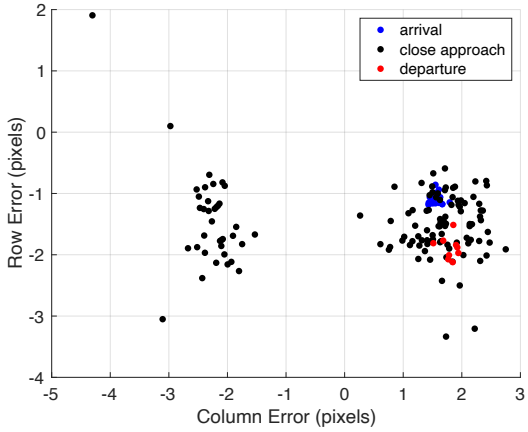

Figure 12. SFN landmark measurement column and row pixel error during first Mercury flyby test.

Lastly, we show the relationship between correlation score and the landmark emission (Figure 13) and incidence (Figure 14) angles for this flyby. Despite establishing above in the science orbit results that correlation score was higher in the ~55 to 75 deg range of incidence angles, Figure 13 seems to suggest a different trend: that values between 70 to 85 deg are even better. However, it must be remembered that the flyby represented a limited geometry of viewing conditions, and because the landmarks were manually selected in each image, there was a preference to place them near the terminator causing the upper right of Figure 13 to be sampled more than in Figure 8. In general, care should be taken in drawing general trends from this limited set of data in Figures 13 and 14 for a single flyby.

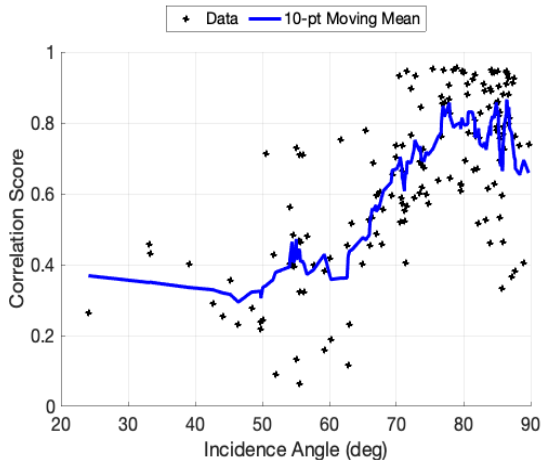

Figure 13. SFN landmark measurement correlation score vs. incidence angle, during first Mercury flyby test.

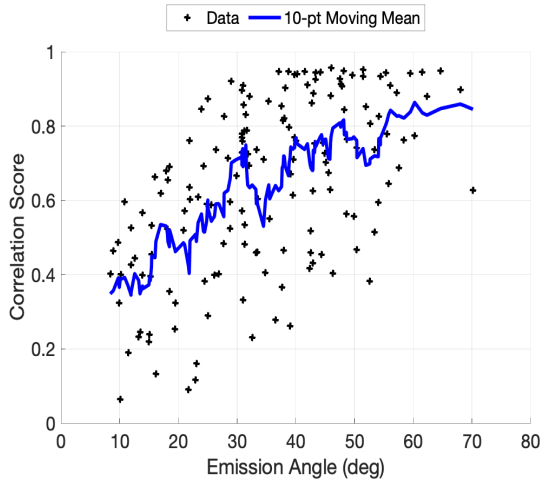

Figure 14. SFN landmark measurement correlation score vs. emission angle, during first Mercury flyby test.

Conclusions and Future Work. Using MESSENGER images and the most up to date SPICE kernels, Mercury surface features are created for the first Mercury flyby and portions of the science orbit. An updated surface feature processing pipeline is added to GIANT's code base to provide another means to generate landmarks from a geoTIFF DTM file. GIANT SFN functionality is used to both render the predicted template for each surface feature and correlate the template to the predicted surface feature location in its associated image. This process results in updated image coordinates for LOS measurements to be created, along with a correlation score between template and image. The results obtained from this process for both the flyby and science orbit phases were analyzed to find relationships between incident angle, emission angle, LOS pixel error, and correlation score. The roughly 3-week span of the science orbit phase under analysis showed consistent LOS pixel error statistics, with a constant bias of approximately 2 pixels, and a standard deviation of approximately 1 pixel. The flyby showed similar pixel error standard deviation, but with a more complex bias pattern. Factors like MDIS gimbal pointing uncertainty are potential sources of this apparent bias that need further analysis. Despite this apparent bias, the standard deviation of approximately 1 pixel error in the row and column components is a promising value that demonstrates the ability of GIANT for generating MESSENGER SFN measurements for processing in a navigation filter. In the future, these SFN measurements can be ingested into a navigation filter to generate both ephemeris files and uncertainty measurements of the MESSENGER spacecraft, which can be compared with definitive best-fit ephemerides. Reducing (or addressing in the filter) the apparent bias in these measurements will be one future obstacle to overcome. Additionally, the SFN measurements show the suitability of using a global Mercury DTM for performing SFN. Compared to the method of using SPC to build large sets of features first, the updated pipeline uses the global DTM as a foundation first, providing an efficient way to generate sets of maplets simultaneously. This method could prove useful in planetary OpNav for planets with existing global DTMs. Development and analysis will continue with the purpose of further maturing the functionality of GIANT to provide an even stronger foundation in future OpNav planetary applications.

References

[1] Bolles, Dana. "Terrain Relative Navigation: Landing Between The Hazards." *NASA Science*, NASA, 15 Feb. 2021. https://science.nasa.gov/technology/technology-highlights/terrain-relative-navigation-landing-between-the-hazards

[2] C. Gnam, A. Liounis, B. Ashman, K. M. Getzandanner, J. Lyzhoft, J. Small, D. Highsmith, C. Adam, J. Leonard, P. Antreasian, and D.S. Lauretta, "A Novel Surface Feature Navigation Algorithm Using Ray Tracing," in 2nd Annual RPI Space Imaging Workshop, Saratoga Springs, NY, Oct. 2019.

[3] Barnett, Amanda. "In Depth: MESSENGER." *NASA Science*, NASA, 1 Aug. 2019. https://solarsystem.nasa.gov/missions/messenger/in-depth/

[4] K. E. Williams, A. H. Taylor, D. R. Stanbridge, P. J. Wolff , B. R. Page, and B. G. Williams, "Navigation For The MESSENGER Mission's First Mercury Encounter," in AIAA/AAS Astrodynamics Specialist Conference and Exhibit, Honolulu, Hawaii, Aug. 2008.

[5] Planetary Data System Image Atlas, NASA Jet Propulsion Laboratory, https://pds-imaging.jpl.nasa.gov/search/, accessed May 2022

[6] National and Ancillary Information Facility, NASA Jet Propulsion Laboratory, https://naif.jpl.nasa.gov/naif/

[7] A.J. Liounis, J. Swenson, J. Small, J. Lyzhoft, B. Ashman, K. Getzandanner, D. Highsmith, M. Moreau, C. Adam, P. Antreasian, and D.S. Lauretta, "Independent Optical Navigation Processing For The OSIRIS-REx Mission Using The Goddard Image Analysis And Navigation Tool ," in 2nd Annual RPI Space Imaging Workshop, Saratoga Springs, NY, Oct. 2019.

[8] A.J. Liounis, C. Gnam, J. Swenson, K. Getzandanner, J. Small, and J. Lyzhoft, (2022). The Goddard Image Analysis and Navigation Tool (Version 1.0.3) [Computer software].

[9] K. Becker, et al., "First Global Digital Elevation Model of Mercury", 47th Lunar and Planetary Science Conference, 2016.

[10] J. Smith, W. Taber, T. Drain, S. Evans, J. Evans, M. Guevara, W. Schulze, R. Sunseri, and H. Wu, "MONTE Python For Deep Space Navigation," in Proceedings of the 15th Python in Science Conference, Jul. 2016, pp. 62 - 68. DOI: 10.25080/Majora-629e541a-009.

[11] J.A. Christian, "Accurate Planetary Limb Localization for Image-Based Spacecraft Navigation," *JSR*, 54(3), 2012, pp. 708-730. DOI: 10.2514/1.A33692.

[12] M. Shoemaker, C. Wright, A. J. Liounis, K. M. Getzandanner, J. M. Van Eepoel, and K. D. DeWeese, "Performance Characterization of a Landmark Measurement System for ARRM Terrain Relative Navigation" in AAS/AIAA Space Flight Mechanics Meeting, Napa, CA, Feb. 2016.

[13] A. Liounis et al., "A Comparison of Bearing Measurements to Surface Features Generated using Stereophotoclinometry and Surface Feature Navigation Techniques" in AAS 12-114

[14] "Mercury Messenger Global Dem 665m V2: USGS Astrogeology Science Center." Mercury MESSENGER Global DEM 665m v2 | USGS Astrogeology Science Center, 21 Oct. 2016, https://astrogeology.usgs.gov/search/map/Mercury/Topography/MESSENGER/Mercury_Messenger_USGS_DEM_Global_665m_v2.

[15] GDAL/OGR contributors (2022). GDAL/OGR Geospatial Data Abstraction software Library. Open Source Geospatial Foundation. URL https://gdal.org

[16] N. Chabot, "MESSENGER MDIS Data Users' Workshop 2013", https://pds-imaging.jpl.nasa.gov/software/Chabot_overview_MDIS_workshop_Ver2.pdf, accessed Sep 12, 2022.